Polarization correlations in pulsed, vertical-cavity, surface-emitting lasers

D.R. Shelly, T.W.S. Garrison, M. Beck
Department of Physics, Whitman College, Walla Walla, Washington 99362
shellydr@whitman.edu, garristw@whitman.edu, beckmk@whitman.edu

D.H. Christensen
National Institute of Standards and Technology, Boulder, Colorado 80303
christen@boulder.nist.gov

Abstract: We have examined the noise behavior and polarization correlations in the output of a pulsed vertical-cavity, surface-emitting laser (VCSEL). We have measured the output of the laser simultaneously in two orthogonal, linear polarizations as a function of drive current for pulse widths of 3 ns, 10 ns, and 30 ns. We present joint probability distributions for the number of detected photoelectrons in each of the two polarization-resolved outputs. The joint distributions indicate that the correlations can be quite complicated, and are not completely described by a single number (i.e., the correlation coefficient). Furthermore, we find that the number of lasing modes appears to be the most important parameter in determining the degree of polarization correlation.

OCIS codes: (250.7260) Vertical cavity surface emitting lasers; (140.5960) Semiconductor lasers

1. Introduction

Vertical-cavity, surface-emitting lasers (VCSELs) are microcavity semiconductor lasers which emit perpendicular to the substrate plane. Largely because of their small size, VCSELs exhibit a number of interesting properties: single-longitudinal mode output, low threshold-current, and high efficiency [1]. However, because of their circular symmetry, polarization selection is very weak in these lasers; consequently the output from a VCSEL is usually not polarized. The details of this polarization behavior are not yet completely understood, and in the past few years there has been a great deal of interest, both experimental and theoretical, in this topic [2-891112131415].

Many previous studies have examined noise and/or polarization behavior of VCSELs, but the vast majority of these experiments have been carried out on continuous-wave (CW) lasers [2-8], while very few have been done using pulsed lasers [9-11]. Here we examine the behavior of a pulsed VCSEL. Furthermore, most previous noise measurements have involved using radio-frequency (RF) spectrum analysis, a technique that essentially measures the variance of the photocurrent fluctuations. To our knowledge all previous quantitative measures of polarization correlations have involved the determination of a correlation coefficient, which is also essentially a second order moment of the intensity fluctuations. Here we have measured not just moments, but the full joint probability distributions for the fluctuations in two orthogonal laser polarizations.

In our experiments we simultaneously detect the two orthogonal polarizations of the light emitted by a VCSEL. The light from each polarization is incident on separate photodetectors, and we measure the number of photoelectrons generated in each detector as a function of drive current. The fact that we make simultaneous measurements on the two polarizations is what allows us to determine the full joint statistics. We find that in general the fluctuations in the orthogonal polarizations are anticorrelated, an observation that has been made previously by others and ourselves [4-8,11]. However, we also find that the polarization correlations can be quite complicated, the joint distributions display considerable non-Gaussian structure, so measurements of second order moments are not enough to fully characterize the correlations.

2. Experiments

For these experiments we used a proton-implanted, gain-guided VCSEL with a peak emission wavelength at 837 nm; it had a 20 μm diameter, current-confined implant region, and an emission aperture of 15 μm. We drove the laser with a series of short (3, 10, or 30 ns) current pulses at a pulse repetition frequency of 20 kHz. The VCSEL had a DC bias of 1.38 V, which we applied through a bias tee. Biasing dramatically reduced ringing, and 1.38 V was the highest voltage we could apply without generating measurable CW background light from the laser; such background was found to increase the noise of our measurements [9].

As is shown in Figure 1, the light from the VCSEL is first collimated by a 10X, 0.25-N.A. microscope objective. It passes through a half-wave plate and then through a polarizing beam-splitter. We adjust the waveplate by driving the laser just above threshold and maximizing the 0^o photodetector output voltage on an oscilloscope. The laser operates in a single, linear polarization near threshold, so the direction of this polarization is what we refer to as 0^o. The light in each polarization exiting the beam-splitter is detected simultaneously by two photodetectors.

The details of our detection system and its calibration are discussed in Ref. [9]. The only difference between our current implementation and that of Ref. [9] is that we now use a 16-bit resolution A/D converter that simultaneously samples two detectors. This higher resolution digitization obviates the need for the biased amplifier we used previously. After calibration, this detection system yields the number of photoelectrons generated by each detector for each laser pulse. We expect this photoelectron number to accurately reflect the number of photons emitted by the laser to within our overall detection efficiency of over 80%.

For each laser pulse width (3.1 ns, 10 ns, and 30 ns), we stepped through drive currents with values from below threshold to values of up to 6 times threshold. For the 30 ns pulses, we attenuated the laser output with a 0.5 ND filter in order to avoid saturating our detectors at higher currents. At each current value we simultaneously recorded the number of generated photoelectrons for each polarization (n_0 and n_{90}, where the subscripts refer to the polarization) for 10^6 pulses. From this data we generated two-dimensional histograms which represent joint probability distributions for the photoelectron numbers in the 0° and 90° polarizations. We use 128 bins along each coordinate, and the histogram bin widths are δn_0 and δn_{90}. We normalized the histograms according to

$$\sum_{n_0}\sum_{n_{90}} P(n_0, n_{90})\delta n_0 \delta n_{90} = 1 \ , \tag{1}$$

so $P(n_0, n_{90})$ represents a joint probability density. These joint distributions, displayed as contour plots, provide a great deal of information about the correlations between the 0º and 90º outputs. Furthermore, from these distributions we calculated the marginal probability densities $P(n_0)$, $P(n_{90})$, $P(n_t)$, where the subscript *t* refers to the total number of photoelectrons $n_t = n_0 + n_{90}$. We also calculated the mean $\langle n \rangle$ and variance $\langle (\Delta n)^2 \rangle$ of n_0, n_{90} and n_t.

To further quantify the correlations between the number of photoelectrons generated in the 0º and 90º polarizations, we calculated a correlation coefficient for these outputs at each drive current. The correlation coefficient is defined as

$$C_{0,90} = \frac{\langle (n_0 - \langle n_0 \rangle)(n_{90} - \langle n_{90} \rangle) \rangle}{\sigma_0 \sigma_{90}} = \frac{\langle n_0 n_{90} \rangle - \langle n_0 \rangle \langle n_{90} \rangle}{\sigma_0 \sigma_{90}} \ , \tag{2}$$

where σ_0 and σ_{90} are the standard deviations of the photoelectron output in each polarization. The correlation coefficient quantifies how the outputs in the two polarizations vary with respect to each other from pulse to pulse. It takes on values $-1 < C_{0,90} < 1$, with $C_{0,90} = 0$ corresponding to no correlation between the two outputs, $C_{0,90} = 1$ corresponding to perfect correlation, and $C_{0,90} = -1$ corresponding to perfect anticorrelation.

In order to determine the structure of the transverse modes of the laser, we measured its frequency spectrum with a scanning Fabry-Perot spectrum analyzer. The spectrum analyzer had a free spectral range (FSR) of 750 GHz and a finesse of greater than 280, yielding a resolution of 2.7 GHz. By placing the spectrum analyzer after the polarizing beamsplitter, with proper adjustment of the λ/2 plate we were able to sequentially measure spectra for each individual polarization output, and the total output. To measure the spectrum of the total output, we rotated the half-wave plate halfway between the settings used to measure the two individual polarizations. Thus, each laser polarization is incident on the polarization axis of the beamsplitter at 45°, and we effectively measure half the output from each polarization. We collected spectra as a function of the laser drive current, and used this data to determine the number of lasing modes at each drive current.

3. Results for 10 ns pulses

Figure 2(a) shows the mean number of detected photoelectrons $\langle n \rangle$ plotted as a function of laser drive current for 10 ns current pulses; these plots are essentially the LI (light-current) curves for our laser. We plot $\langle n \rangle$ for each polarization and the total. As can be seen from the

figure, the light output does not increase linearly with current but rather has kinks. Such behavior has been observed before, and these kinks correspond to points where an additional mode comes above threshold [2,9]. The arrows in Fig. 2 indicate current values where a new laser mode comes above threshold. These points were determined by examining the laser spectra. At each arrow one new mode comes above threshold, and we have labeled the polarization of the new mode (0^o or 90^o) at the arrow. Thus, there's one mode lasing in the 0^o polarization between 3.0 and 3.x mA, while there are two modes in the 0^o polarization and two modes in the 90^o polarization between x and y mA. Above 6.6 mA it becomes difficult to resolve the mode structure, and the best we can say is that there are 6 or more modes lasing.

In Fig. 2(b) we plot the variance of the detected photoelectrons $\left\langle (\Delta n)^2 \right\rangle$ plotted as a function of laser drive current for 10 ns current pulses, again showing data for each polarization and the total. It can bee seen that there are sudden increases in photon variance when a new mode turns on. Such increases have been observed before, and are associated with increases in mode partition noise with the turn-on of additional modes [4,11]. Another interesting feature of Fig. 2(b) is that $\left\langle (\Delta n)^2 \right\rangle$ is larger for the individual polarizations than it is for the total output. The only way this can occur is if the outputs in the two polarizations are anticorrelated. This behavior has been observed previously by us and by others, and can be explained as competition between modes in the two polarizations for a fixed amount of total gain [4-8,11]. The total output is fixed by the total available gain, but the distribution of this output between the two polarizations is not so tightly constrained. Thus, the total output fluctuates less than the outputs in the individual polarizations.

The primary purpose of our experiments was to explore in more detail the correlations between the laser polarizations. As described above, we accomplished this by examining distributions, which measure the joint probability density $P(n_0, n_{90})$ that there will be n_0 photoelectrons generated in the detector monitoring the 0^o polarization and n_{90} photoelectrons in the detector monitoring the 90^o polarization. Fig. 3 shows an example of a typical two-dimensional distribution and its relationship to the 1-dimensional marginal distributions. For example, the 1D distribution for the 90^o polarization can be formed by integrating out the 0^o information, that is integrating along vertical lines in Fig. 3(a) and essentially projecting it onto the horizontal axis. For our discrete distributions this means performing the sum

$$P_{90}(n_{90}) = \sum_{n_0} P(n_0, n_{90}) \delta n_0 \ . \tag{3}$$

This distribution is plotted in Fig. 3(b). Similarly, $P_{90}(n_{90})$, Fig. 3(c), can be formed by integrating out the 90^o information, i.e., projecting the 2D distribution onto the vertical axis. It so happens that the distribution for the total output $P_t(n_t)$, Fig. 3(d), can be found by integrating along lines that make a slope of -1 in Fig. 3(a), and thus projects the joint distribution onto an axis that makes a 45^o angle.

The shape of the 2D joint distributions gives direct evidence for anticorrelation between the 0^o and 90^o outputs, as we find that above threshold, these distributions lie primarily along a line whose slope is –1. Anticorrelation tells us that light pulses that have a higher n_{90} will tend to have a lower n_0, and vice versa. This is shown clearly in Fig. 3(a); at this drive current of 9.5 mA there are more than six modes lasing, and the anticorrelations are very strong.

We also constructed QuickTime animations of the 2D joint distributions, displayed with increasing drive current in time; these are shown in Fig. 4. These animations show how the distributions change in size, shape, and position with increasing drive current. Figure 4(a)

shows how the shape of the idstributions change with drive current. It will be noticed that at lower currents, corresponding to small numbers of lasing modes, the distributions tend to be asymmetric and can be non-Gaussian. However at larger currents the distributions become symmetric Gaussian distributions, which lie predominantly along a line whose slope is -1, which indicates strong anticorrelation between the polarization outuputs. It will also be noticed that at certain currents there are qualitative changes in the shape of the distributions. By comparing with Fig. 2, it will be seen that these changes usually occur at currents where a new mode comes above threshold.

Figure 4(b) shows animations that are derived from exactly the same data as in Fig. 4(a), but the frames are plotted on a much larger scale. Here the scale is large enough to include the entire evolution of distribution, from the smallest current to the largest. This figure illustrates how the mean number of photoelectrons $\langle n \rangle$ changes in each polarization, as well as how the shape and size of the distribution changes, as a function of drive current. The drawback to this animation is that at low drive currents the distributions themselves are so small that they can barely be seen. For full benefit of Fig. 4, both animations should be played simultaneously, side by side.

Figure 5 shows a plot of the correlation coefficient $C_{0,90}$ as a function of drive current for 10 ns pulses. Again, arrows indicate currents where new modes come above threshold. As can be seen, when the laser is below threshold the two polarizations are slightly positively correlated. We believe that this is due to small fluctuations in the pump current; such fluctuations would affect the number of emitted photons in both polarizations in the same way, and thus the two outputs would be positively correlated.

Once the laser comes above threshold (in the 0^o polarization) at 3.0 mA, the correlation coefficient drops dramatically and the two polarizations become strongly anticorrelated. However, when the second mode turns on at 3.4 mA (also in the 0^o polarization), the outputs become less anticorrelated. We hypothesize that this behavior is due to the fact that much more light is being emitted in the 0° polarization, since none of the 90° polarization modes are yet lasing. The relatively high output in the 0° polarization causes much larger fluctuations in this polarization than in the 90° polarization. Thus, the 90° fluctuations are unable to compensate for the 0° fluctuations and the anticorrelation between the two outputs decreases. In other words, there simply isn't enough intensity in the 90^o polarization to develop any significant correlation.

When the third mode (the first in the 90° polarization) turns on at 4.0 mA, the output becomes slightly more anticorrelated, and when the fourth mode (the second 90°) turns on at 4.5 mA the output becomes significantly more anticorrelated, approaching a perfect anticorrelation of $C_{0,90}$ = -1. This is expected, since the fourth mode is much stronger and once it turns on, the number of photoelectrons in the two polarizations becomes similar. At very high currents the outputs become slightly less anticorrelated.

Figure 5 clearly shows that the number of lasing modes in this laser dramatically effects the polarization correlations, since abrupt changes in the correlation coefficient occur precisely at currents where new laser modes come above threshold. This is consistent with the observations made regarding Fig. 4 in which qualitative changes in the shape of the joint distributions are associated with changes in number of lasing modes.

4. Results for other pulse widths

In addition to studying 10ns pulses, we repeated the above-described experiments with drive-current pulse widths of 3 and 30 ns. Differences in the behavior of the laser between these three pulse widths indicate how the laser behaves on different timescales. In Fig. 6 we show animations of the joint probability densities $P(n_0, n_{90})$ for 3 and 30 ns duration pulses. because shorter pulses contain fewer photons, we were able to drive the 3 ns pulses higher

above threshold than the longer pulses, and it can be seen that at higher drive currents the joint distributions for the 3 ns long pulses take on some interesting shapes. By comparing the shapes of the distributions for the three different pulsewidths closer to threshold, it can be seen that the distributions for shorter pulses tend to have more irregular shapes, while those of the longer pulses tend to be smoother.

We find that as the pulse width changes, so does the amount of polarization correlation. In Fig. 7 we plot the correlation coefficient for each pulse width as a function of normalized current (drive current divided by the threshold drive current). We have chosen to use this normalized horizontal scale because while the 10ns and 30 ns pulses have similar threshold currents, the 3 ns pulses have a higher threshold current. This is because the rise and fall times of our pulses are approximately 2.5 ns, which means that the 3 ns current pulses are not square. As can be seen from Fig. 7, all pulse widths display roughly the same qualitative behavior. In the region between about 1.2 and 1.7 times threshold, it is seen that the polarization anticorrelations are stronger for shorter pulses. As stated above, we believe that the reason that correlations decrease in this region is due to the large imbalance in the intensities of the two polarizations. This imbalance is more pronounced for longer pulses, so it stands to reason that if this explanation is correct that longer pulses would have weaker correlations in this region.

In Fig. 8, we plot the relative noise RN of the laser output as a function of the normalized current for the three different pulsewidths. The relative noise is defined as [9]

$$RN = \frac{\langle (\Delta n_t)^2 \rangle}{\langle n_t \rangle^2} \quad . \tag{4}$$

As can be seen, the shorter pulses tend to be noisier. One possible explanation for this is that transients increase the noise early in the pulse; when these transients die out the pulse displays lower-noise, more steady state operation.

5. Conclusions

We have measured the polarization correlations of a pulsed VCSEL. Above threshold, the outputs in the orthogonal, linear polarizations of the laser are anticorrelated. We also find that the degree of correlation depends primarily upon the number of lasing modes. Anticorrelation is greatest when a) the outputs in the two polarizations are of similar amplitude and b) many modes are lasing. These criteria are plausible because anticorrelation depends upon competition between the modes of the two polarizations. A very weak output cannot compete well with a strong output. Also, mode competition that leads to anticorrelation depends upon spatial and temporal overlap of the modes in the laser. The more modes that are lasing in the two polarizations, the more likely these modes are to overlap and affect each other through spatial holeburning.

Although we can quantify the polarization correlations by the correlation coefficient $C_{0,90}$, we find that this is a drastic oversimplification of the problem. The correlation coefficient is derived from second order moments of the joint probablity density for the polarization fluctuations $P(n_0, n_{90})$. For Gaussian statistics, moments up to second order can fully characterize the fluctuations; to a good approximation this is the case for our laser when it is between 1.8 and 5 times above threshold. However, closer to threshold we find that the statistics are not Gaussian (Figs. 4 & 6), and the correlations are of a much more complicated form. [

We also have indirect evidence that the noise of the laser changes in time. This comes from the observation that the relative noise of shorter laser pulses is larger than that of longer laser pulses; which suggests larger noise right after the laser turns on followed by quieter

operation. In order to more fully describe this behavior, more detailed experiments to better time-resolve the fluctuations are necessary.

Acknowledgments

M. Beck is a Cottrell Scholar of the Research Corporation. Further support for this work came from the National Science Foundation.

References and links

1. C. J. Chang-Hasnain, "Vertical-cavity surface emitting lasers," in *Semiconductor Lasers: Past, Present, and Future*, G. P. Agrawal, ed. (American Institute of Physics, Melville, N.Y., 1995), pp. 145-180.
2. F. Koyama, K. Morit, and K. Iga, "Intensity noise and polarization stability of GaAlAs-GaAs surface emitting lasers," IEEE J. Quantum Electron. **27**, 1410-1416 (1991).
3. T. Mukaihara, N. Ohnoki, Y. Hayashi, N. Hatori, F. Koyama, and K. Iga, "Excess intensity noise originated from polarization fluctuation in vertical-cavity surface-emitting lasers," IEEE Photon. Technol. Lett. **7**, 1113-1115 (1995).
4. D.C. Kilper, P.A. Roos, J.L. Carlsten, and K.L. Lear, "Squeezed light generated by a microcavity laser," Phys. Rev. A **55**, R3323-R3326 (1997).
5. M.P. van Exter, M.B. Willemsen, and J.P. Woerdman, "Polarization fluctuations in vertical-cavity semiconductor lasers," Phys. Rev. A **58**, 4191-4205 (1998).
6. G. Giacomelli, F. Martin, M. Gabrysch, K.H. Gulden, and M. Moser, "Polarization competition and noise properties of VCSELs," Opt. Comm. **146**, 136-140 (1998).
7. J.-L. Vey, C. Degen, K. Auen, and W. Elsäßer, "Quantum noise and polarization properties of vertical-cavity, surface-emitting lasers," Phys. Rev. A **60**, 3284-3295 (1999).
8. M.B. Willemsen, M.P. van Exter, and J.P. Woerdman, "Correlated fluctuations in the polarization modes of a vertical-cavity semiconductor laser," Phys. Rev. A **58**, 4191-4205 (1998).
9. D.V. Kuksenkov, H. Temkin, and S. Swirhun, "Polarization instability and relative intensity noise in vertical-cavity surface-emitting lasers," Appl. Phys. Lett. **67**, 2141-2143 (1995).
10. D.V. Kuksenkov, H. Temkin, and S. Swirhun, "Polarization instability and performance of free-space optical links based on vertical-cavity surface-emitting lasers," IEEE Photon. Technol. Lett. **8**, 703-705 (1996).
11. T.W.S. Garrison, M. Beck, and D.H. Christensen, "Noise behavior of pulsed vertical-cavity, surface-emitting lasers," J. Opt. Soc. Am. B **16**, 2124-2130 (1999).
12. K.D. Choquette, R.P. Schneider, and K.L. Lear, "Gain-dependent polarization properties of vertical cavity lasers," IEEE J. Select. Topics Quantum Electron. **1**, 661-666 (1995).
13. M. San Miguel, Q. Feng, and J.V. Molony, "Light-polarization dynamics in surface-emitting semiconductor lasers," Phys. Rev. A **52**, 1728-1739 (1995).
14. A. Valle, L. Pesquera, and K.A. Shore, "Polarization behavior of birefringent multitransverse mode vertical-cavity surface-emitting lasers," IEEE Photon. Tech. Lett. **9**, 557-559 (1997).
15. K. Panajotov, B. Kyvkin, J. Danckaert, M. Peeters, H. Thienpont, and I. Veretennicoff, "Polarization switching in VCSEL's due to thermal lensing," IEEE Photon. Tech. Lett. **10**, 6-8 (1998).

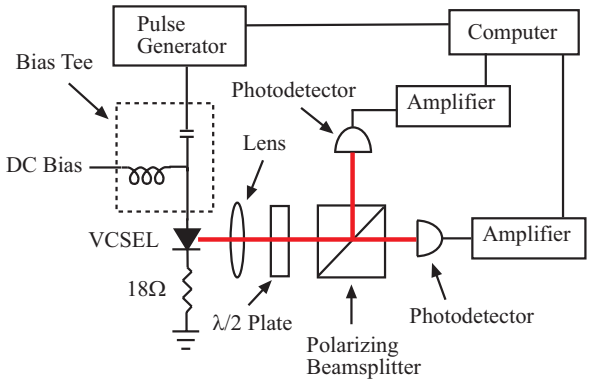

Fig. 1 The expt. apparatus.

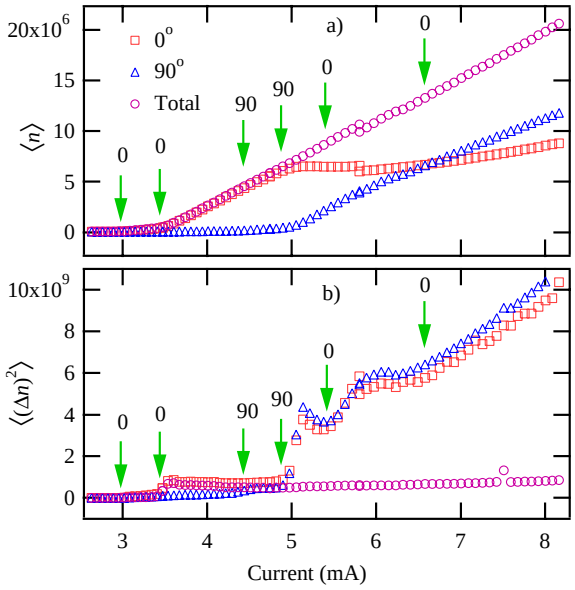

Fig. 2 LI and Variance

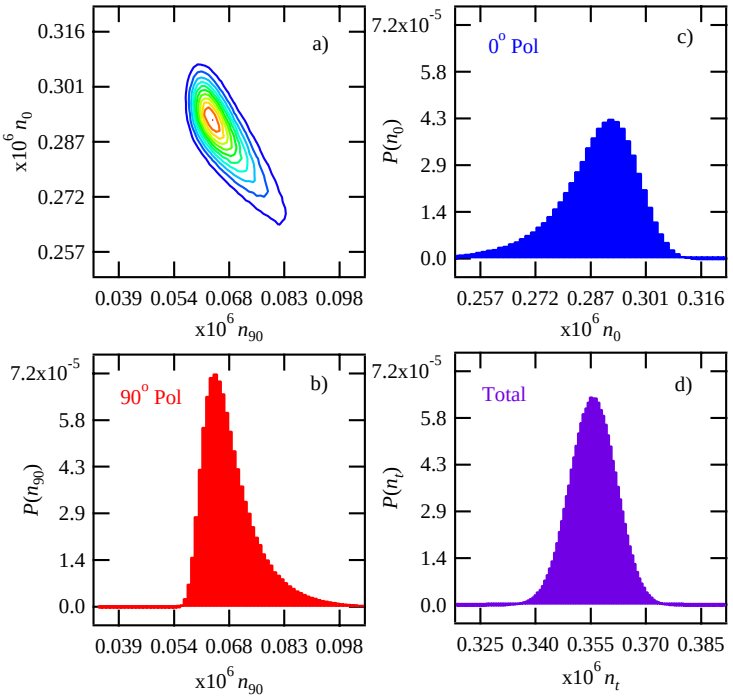
a)
0.316
0.301
0.287
0.272
0.257
x10^6 n0
0.039 0.054 0.068 0.083 0.098
x10^6 n90
7.2x10^-5
0° Pol
c)
5.8
4.3
2.9
1.4
0.0
P(n0)
0.257 0.272 0.287 0.301 0.316
x10^6 n0
b)
90° Pol
P(n90)
d)
Total
P(nt)
0.325 0.340 0.355 0.370 0.385
x10^6 nt

Fig. 3

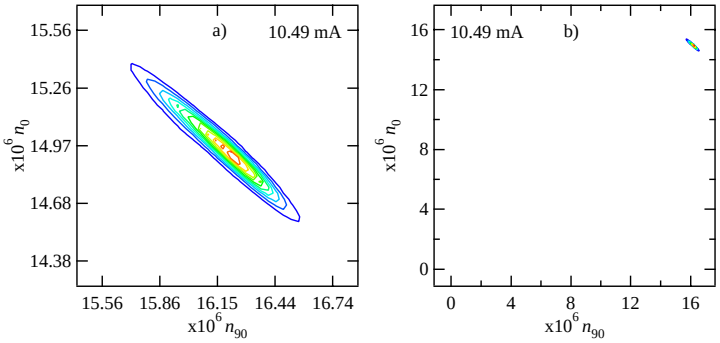
a)
10.49 mA
15.56
15.26
14.97
14.68
14.38
x10^6 n0
15.56 15.86 16.15 16.44 16.74
x10^6 n90
b)
16
12
8
4
0
0 4 8 12 16

Fig 4

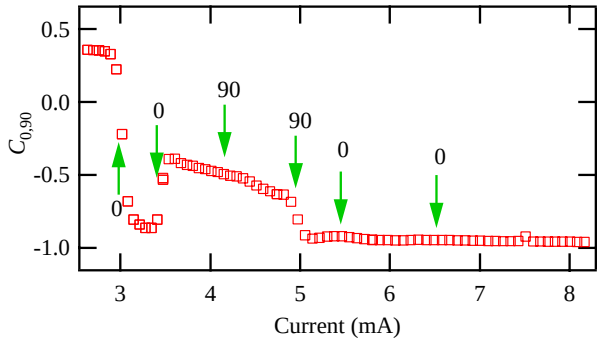
0.5
0.0
-0.5
-1.0
C0,90
0
90
90
0
0
0
3 4 5 6 7 8
Current (mA)

Fig. 5

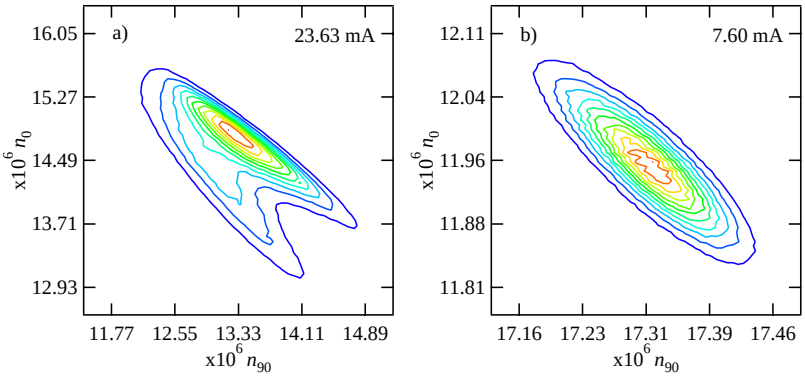

fig. 6

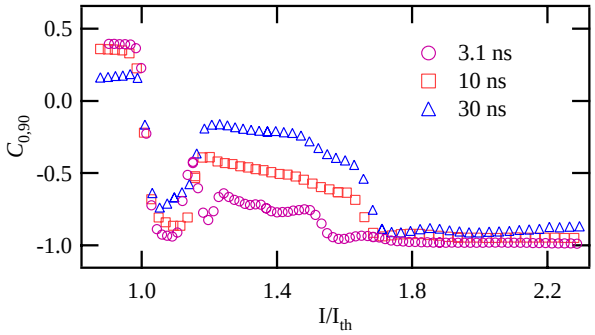

Fig. 7

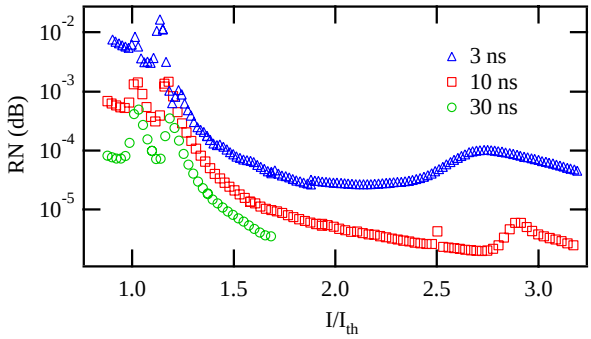

Fig. 8